Tunable Electrical and Thermal Transport in Ice-Templated Multilayer Graphene Nanocomposites through Freezing Rate Control

Scott N. Schiffres,[†,⊥] Sivasankaran Harish,[‡,⊥] Shigeo Maruyama,[‡] Junichiro Shiomi,[‡,∥] and Jonathan A. Malen[†,§,*]

[†]Department of Mechanical Engineering, Carnegie Mellon University, 5000 Forbes Avenue, Pittsburgh, Pennsylvania 15213, United States, [‡]Department of Mechanical Engineering, The University of Tokyo, 7-3-1 Hongo, Bunkyo-ku, Tokyo 113-8656, Japan, [§]Department of Material Science & Engineering, Carnegie Mellon University, 5000 Forbes Avenue, Pittsburgh, Pennsylvania 15213, United States, and [∥]CREST, Japan Science and Technology Agency, Chiyoda, Tokyo 102-0075, Japan. [⊥]S. N. Schiffres and S. Harish contributed equally to this work.

ABSTRACT We demonstrate tunable electrical and thermal conductivities through freezing rate control in solution-based nanocomposites. For a prototypical suspension of 1 vol % multilayer graphene suspended in hexadecane, the solid–liquid electrical conductivity contrast ratio can be tuned from 1 to 4.5 orders of magnitude for freezing rates between 10^2 and 10^{-3} °C/min. We hypothesize that this dramatic variation stems from ice-templating, whereby crystal growth drives nanoparticles into concentrated intercrystal regions, increasing the percolation pathways and reducing the internanoparticle electrical resistance. Optical microscopy supports the ice-templating hypothesis, as these dramatic property changes coincide with changing crystal size. Under the same range of freezing rates, the nanocomposite solid–liquid thermal conductivity contrast ratio varies between 2.3 and 3.0, while pure hexadecane's varies between 2.1 and 2.6. The nanocomposite's thermal conductivity contrast ratios and solid phase enhancements are greater than effective medium theory predictions. We suggest this is due to ice-templating, consistent with our electrical measurements, as well as nanoparticle-induced molecular alignment of alkanes.

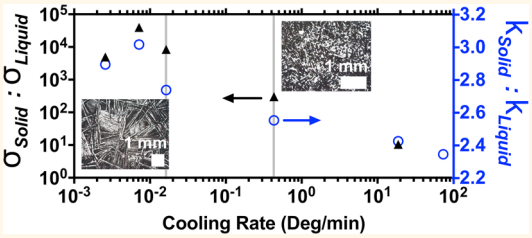

KEYWORDS: phase change nanocomposite · ice-templating · tunable electrical conductivity · tunable thermal conductivity · freezing rate dependence · multilayer graphene · hexadecane

Solution-based nanoparticle composite materials promise scalability for diverse energy technologies, yet challenges persist in the control of nanoparticle network morphology, as well as the resulting electrical and thermal conductivities. Morphological control of these transport properties has scientific and technological importance, with applications to electrical energy storage,[1−3] thermal energy storage,[4−13] and composite materials.[14−21] Ice-templated materials are freeze-cast composites that possess intricate structures on multiple length scales, ranging from nanometers to millimeters.[22] These multiple length scales emerge when the base fluid solidifies into snowflake-like crystals, driving or "templating" the nanoparticles into the intercrystal region.[22] For example, ice-templated biomimetic seashell nacre is reported to have enhanced mechanical properties derived from the intricate microstructuring, but the effect of ice-templating on electrical and thermal properties remains unexplored.

Controllable transport properties in phase change nanocomposites can benefit applications in thermal and electrical energy storage. Phase change thermal storage seeks to reduce building heating and cooling energy consumption by moderating temperature swings and compensating for temporal offsets in energy supply and demand.[6] Thermal energy storage is also an appealing way to cool power electronics during peak loads[7,8] and to store off-peak thermal energy in industrial processes.[9−11,23,24] In melting or freezing, the thermal energy storage rate is proportional to the phase change material's thermal conductivity.[4] Room-temperature phase change materials, such as alkanes, possess poor thermal conductivity, which limits the energy storage

* Address correspondence to jonmalen@andrew.cmu.edu.

Received for review September 21, 2013 and accepted November 6, 2013.

Published online November 06, 2013
10.1021/nn404935m

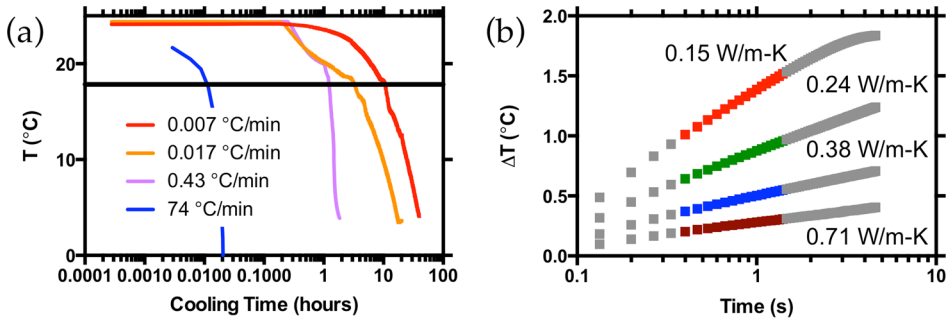

Figure 1. (a) Representative plots of sample cooling *versus* time on a logarithmic scale. The fastest freezing (blue) was liquid nitrogen cooled, while others were frozen with a Peltier cooler. The black line is the phase transition temperature for bulk hexadecane of 17.8 °C. (b) Typical transient hot wire thermal conductivity measurement data. The colored region of each line represents the segment of the transient hot wire data used to determine the thermal conductivity. The red, green, blue, and brown data points are for liquid hexadecane, liquid nanocomposite, solid hexadecane, and solid nanocomposite, respectively.

and withdrawal rate. This has led to interest in increasing the thermal conductivity of phase change materials through the addition of high thermal conductivity nanoparticles.[5,12,13,25,26] Tunable properties through phase change could also optimize electrical energy storage through the control of nanoparticle network morphology and electrical conductivity.[1]

Recently, molecular dynamics simulations have predicted that the presence of carbon nanotubes (CNTs) and graphene induces a more orderly alkane crystallization, thereby increasing the thermal conductivity of phase change nanocomposites.[27−29] Order induced near the nanoparticle surface is also reported to reduce the time for crystals to nucleate.[14] Simulations of Babaei *et al.*[29] show that introducing CNTs and graphene to liquid alkane enhances the solid-state thermal conductivity of the alkane significantly compared to its liquid state. This mechanism has been proposed to explain the unexpectedly large solid−liquid thermal conductivity enhancements recently reported using graphite−hexadecane,[4] CNT−octadecane,[11] and CNT−hexadecane suspensions.[9] However, the mechanisms responsible for these unusual solid−liquid thermal conductivity enhancements remains unclear, and its dependence on freezing rate is as yet unknown.

Hence, we seek to understand the electrical and thermal transport properties of phase change nanocomposites by varying the underlying microstructure through the freezing rate. Using multilayer graphene (MLG) nanoplatelet−hexadecane suspensions, we show that slower freezing rates lead to nanocomposites with improved electrical and thermal conductivities. Surprisingly, the electrical conductivity contrast ratio $\sigma_{Solid}/\sigma_{Liquid}$ can be tuned between 1 and 4.5 orders of magnitude, and the solid−liquid thermal conductivity contrast ratio k_{Solid}/k_{Liquid} can be tuned between 2.3 and 3.0 by varying only the freezing rate.

RESULTS AND DISCUSSION

Samples were frozen at rates between 10^{-3} and 10^{2} °C/min (Figure 1a) using Peltier and liquid nitrogen cooling. Temperature, thermal conductivity, and electrical conductivity were measured every minute during freezing. Representative transient hot wire thermal conductivity measurements of temperature rise *versus*

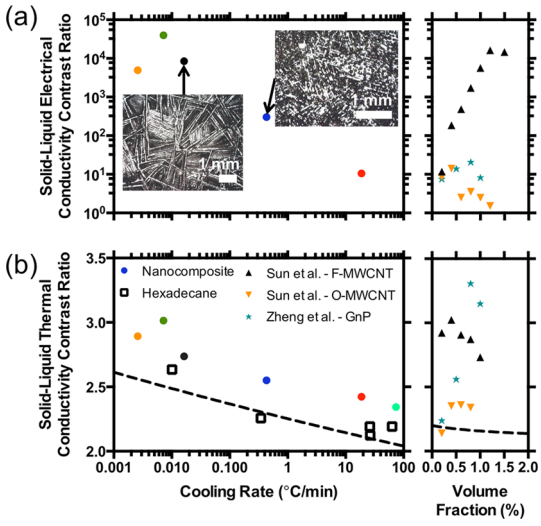

Figure 2. (a) Solid−liquid electrical conductivity contrast ratios ($\sigma_{Solid}/\sigma_{Liquid}$) plotted *versus* cooling rate for the hexadecane with 1 vol % MLG. The mean liquid state electrical conductivity is 0.02 μS/cm at 24 °C. Solid measurements were taken at 5 °C. Inset images of the top surface of the nanocomposite were taken with an optical microscope at the respective cooling rates. The length dependence of crystals with cooling rate is notable. To the right are the solid−liquid electrical contrast ratios achieved by Sun *et al.* and Zheng et al. *versus* volume fraction, as freezing rate was not reported. Sun *et al.* measured suspensions of pristine and antiagglomeration functionalized multiwalled carbon nanotubes (O-MWCNTs and F-MWCNTs) in hexadecane, while Zheng *et al.* measured graphite nanoplatelets (GnP) in hexadecane. (b) The solid−liquid thermal conductivity contrast ratios (k_{Solid}/k_{Liquid}) are plotted *versus* cooling rate for bulk hexadecane (black squares) and for hexadecane with 1 vol % MLG (circles color coded by cooling rate). The average liquid-state thermal conductivity of the liquid nanocomposite and hexadecane are 0.24 and 0.15 W/m-K at 24 °C. The right plot shows the solid−liquid thermal conductivity contrast ratios of Sun *et al.* and Zheng *et al.* *versus* vol %. The dashed lines are the Nan *et al.* effective medium predicted contrast ratios (details are in the Materials and Methods section).

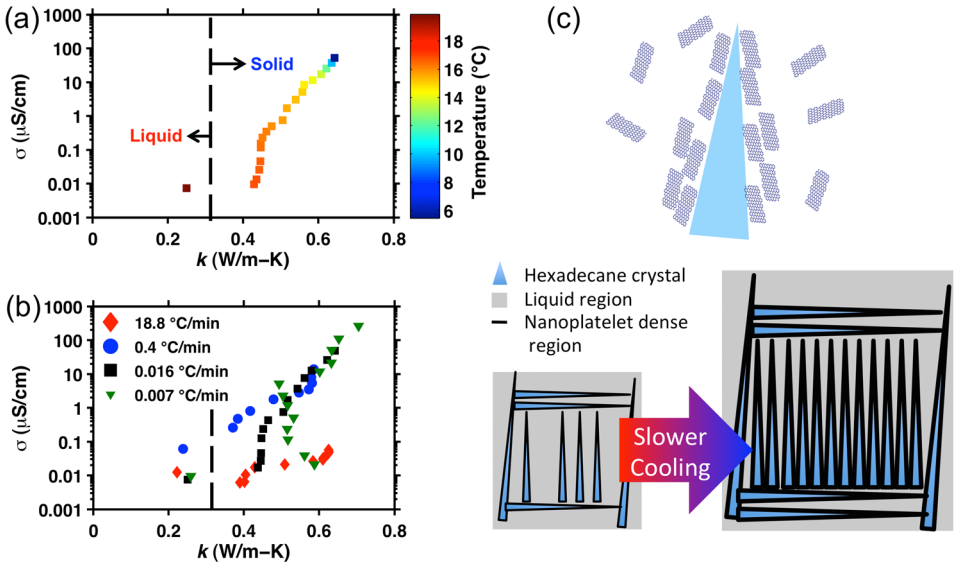

Figure 3. (a) Plots of the electrical *versus* thermal conductivity during a freezing at 0.016 °C/min with each data point's color representing the temperature at that measurement. After freezing there is an exponential increase in electrical conductivity for a linear change in thermal conductivity. (b) Trends for electrical *versus* thermal conductivity taken at various cooling rates showing a similar trend except for the rapid liquid nitrogen cooled data (19 °C/min). The trend shared by the slowest and moderate cooling rates differ primarily in the final extent of enhancement but not in the path to that enhancement *versus* temperature. The liquid nitrogen cooled sample (19 °C/min) does not follow this trend and has less improvement in both electrical and thermal conductivity than the slower cooled measurements. (c) This graphic illustrates our hypothesis that crystal growth drives MLG nanoplatelets to grain boundary and that slower freezing will lead to larger hexadecane crystal growth. We suggest that ice-templating leads to increased electrical percolation pathways and reduced electrical resistance between nanoplatelets, as well as reduced internanoparticle thermal resistance.

time are shown in Figure 1b. Instrumentation and data analysis are further described in the Materials and Methods section. The solid–liquid contrast ratios of electrical and thermal conductivity for hexadecane with 1 vol % MLG nanoplatelets are shown in Figure 2a and b, where liquid properties are at 24 °C and solid properties are at 5 °C (absolute electrical conductivity measurements are plotted in Supporting Information Figure S1). The liquid state has an average electrical conductivity of 0.02 μS/cm (ranging from 0.006 to 0.06 μS/cm) at 24 °C. The minimum $\sigma_{Solid}/\sigma_{Liquid}$ of just 1 order of magnitude was achieved at the rapid cooling rate of 19 °C/min and surged to 4.5 orders of magnitude at the minimum tested cooling rate of 10^{-3} °C/min. The $\sigma_{Solid}/\sigma_{Liquid}$ ratios are greater than reported by Zheng *et al.*, where the $\sigma_{Solid}/\sigma_{Liquid}$ ranged from 50 to 250 times for 0.2 to 1.0 vol % graphite–hexadecane suspensions. Similar $\sigma_{Solid}/\sigma_{Liquid}$ ratios were observed by Sun *et al.* in antiagglomeration functionalized CNTs, while much lower $\sigma_{Solid}/\sigma_{Liquid}$ ratios were observed in nonfunctionalized CNT suspensions (Figure 2a).[4,9]

Liquid hexadecane with 1 vol % MLG nanoplatelets has a thermal conductivity at 24 °C of 0.24 W/m-K, which is 65% greater than liquid hexadecane. The nanocomposite solid–liquid thermal conductivity contrast ratio k_{Solid}/k_{Liquid} can be controlled from 2.3 to 3.0 for freezing rates between 10^{2} and 10^{-3} °C/min, as shown in Figure 2b (absolute thermal conductivity measurements are plotted in Supporting Information Figure S2). For the same range of freezing rates, pure hexadecane k_{Solid}/k_{Liquid} ratio followed a similar trend and varied from 2.1 to 2.6. Our maximum k_{Solid}/k_{Liquid} ratio of 3.0 is near Zheng *et al.*'s published k_{Solid}/k_{Liquid} ratio for 1 vol % graphite nanoplatelets in hexadecane.[4] The nanocomposite thermal conductivity enhancement relative to similarly frozen pure hexadecane k_{NC}/k_{Base} is 1.81 $\pm$ 0.08 over the range of freezing rates, while the nanocomposite liquid precursor suspension relative to pure liquid hexadecane k_{NC}/k_{Base} is 1.65 $\pm$ 0.07.

Paralleling these changes in electrical and thermal conductivity, the nanocomposite develops longer and thicker needle-like patterns with slower freezing, as shown in the insets of Figure 2a. In a process analogous to the ice-templating of a biomimetic seashell, we observe a microstructural change in the nanocomposite with freezing rate.[22] These images reveal that the nanocomposite solidifies through needle-like crystals that are mostly aligned parallel to neighboring needles. Environmental scanning electron microscopy (ESEM) images recorded at 0.5 °C/min reveal the presence of needle-like structures that vanish upon melting (Supporting Information Figure S3). Due to experimental constraints, slower cooled ESEM studies could not be performed.

Measurements of electrical and thermal conductivities through freezing reveal an exponential increase in electrical conductivity for a linear increase in thermal conductivity (Figure 3a). A common trend emerges for

electrical *versus* thermal conductivity when various cooling rates are plotted together (Figure 3b). Moderately and slowly cooled samples differ only in the extent of their thermal and electrical conductivity enhancements, not in the path. Contrastingly, samples frozen more rapidly with liquid nitrogen measure a significantly smaller improvement in both electrical and thermal conductivity through freezing.

Drawing from related research on particle incorporation during metal solidification, the underlying mechanism that propels nanoparticles out of the crystallizing hexadecane is the reduced surface energy of the nanoparticles in the liquid *versus* the solid phase (Figure 3c).[30] This surface energy difference provides the propulsive force pushing the nanoparticles away from the solidification front, but is countered by the viscous drag acting on the nanoparticles traveling through the melt.[30] If the freezing front is moving beyond a critical speed, the drag acting on a nanoparticle will exceed the free-energy gradient driving force, leaving the nanoparticles engulfed in the crystal, rather than concentrated and compressed into the intercrystal region. Larger crystals grown at slower cooling rates will have more nanoparticles accumulated at the intercrystal region, as illustrated in Figure 3c. We hypothesize that the nanoparticle-rich intercrystal region creates additional percolation pathways for electrical conduction and reduced internanoparticle electrical resistance. The analysis that follows suggests that electrical conductivity is highly sensitive to the morphology of the nanoparticle-rich regions due to percolation and the internanoparticle tunneling separation, while thermal conductivity is approximately a linear function of the constituent properties. It follows that the exponential enhancement of electrical conductivity with linear enhancement of thermal conductivity is consistent with crystal growth ice-templating the nanoparticle network concurrent with shifting constituent properties through solidification.

The freezing rate controlled solid−liquid electrical conductivity ratio can be analyzed through percolation theory. Percolation theory for electrical conductivity due to a conductive nanoparticle in an insulating base material is often modeled[31] as

$$\sigma \propto \left(\frac{\phi - \phi_C}{1 - \phi_C}\right)^U \quad (1)$$

where ϕ_C is the critical nanoparticle volume fraction threshold and U is the universal critical exponent. The electrical conductivity contrast ratio predicted from densification of nanoparticles is

$$\frac{\sigma_{Solid}}{\sigma_{Liquid}} \propto \left(\frac{\phi' - \phi_C}{1 - \phi_C}\right)^U \left(\frac{\phi - \phi_C}{1 - \phi_C}\right)^{-U} \left(\frac{\phi}{\phi'}\right) \quad (2)$$

where ϕ' is the volume fraction in the intercrystal high concentration regions.

Using typical values for MLG nanoplatelets' ϕ_C and U values of 0.05−0.1% and 2−3, respectively, the crystals would have to concentrate the nanoplatelets to a volume fraction of greater than 30% to have a solid−liquid electrical conductivity contrast ratio of 4.5 orders of magnitude.[4,31] This densification theory is also supported by Sun *et al.*'s finding that antiagglomeration functionalized multiwalled CNT−hexadecane nanocomposites have much greater solid−liquid contrast ratios than pristine multiwalled CNT−hexadecane nanocomposites, which more readily agglomerate in the liquid state (Figure 2a).[9]

Because the hexadecane is electrically insulating, the nanocomposite electrical conductivity is a function of the internanoplatelet electrical resistance, the nanoplatelet conductance, and the nanoplatelet network morphology. The nanoplatelets' high electrical conductance suggests that the electrical resistance of the internanoparticle junctions will dominate the nanocomposite's electrical properties.[19] The resistance of a tunneling junction increases exponentially with the junction separation ($R_{Elec} \propto R_0 e^{\beta d}$). Rampi *et al.* considered the electrical resistance through various length alkane chains with different end-groups (alkane-thiols, alkane-phenols, *etc.*).[32] While the alkane chemistry characteristic tunneling length, $1/\beta$, depends on end-group chemistry, the range of characteristic lengths stays within a band of 1.15 to 1.64 Å.[32] Under the assumption that the internanoparticle junctions in the percolating network obey similar tunneling behavior, our electrical conductivity enhancement from 1 to 4.5 orders of magnitude can be explained by a reduction in the internanoparticle separation of ∼1 nm between different freezing rates.

Effective medium theory (EMT) is used to predict the thermal conductivity of composite materials based on the thermal conductivities and volume fractions of the continuous base phase and the discontinuous inclusion phase, the thermal boundary conductance, as well as the dimensions and orientation of the inclusions.[33−36] We employed the Nan *et al.* model for randomly oriented ellipsoidal particles, which is further described in the Materials and Methods section.[34]

Our k_{Solid}/k_{Liquid} ratios *versus* cooling rate exceed the EMT predictions, shown as dashed lines in Figure 2b. The k_{Solid}/k_{Liquid} ratios of Sun *et al.* and Zheng *et al.* also exceed these predictions. As a different perspective, Figure 4 compares the experimental and EMT-predicted thermal conductivity enhancement ratios k_{NC}/k_{Base} as a function of base hexadecane thermal conductivity k_{Base}. EMT predicts that k_{NC}/k_{Base} will decrease through freezing because the k_{Base} increases, therefore reducing the impact of higher thermal conductivity nanoparticles. EMT correctly captures ∼80% of the enhancement as being the result of increased base thermal conductivity, which is also evident from the identical hexadecane and nanocomposite k_{Solid}/k_{Liquid}

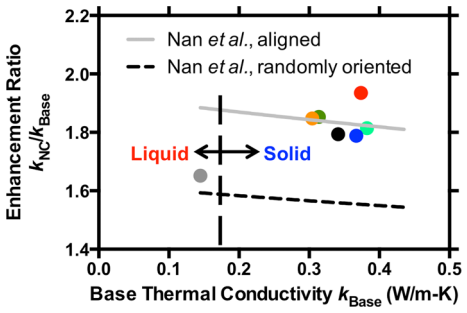

Figure 4. Liquid and solid nanocomposite thermal conductivity enhancements *versus* base material thermal conductivity. The dashed black line is an effective medium prediction of how enhancement should change *versus* base thermal conductivity. We used the Nan *et al.* model for oblate ellipsoidal nanoparticles with random (dashed line) and fully aligned (gray line) orientations, with details on the EMT model in the Materials and Methods.

trends in Figure 2b. Nonetheless, the remaining ~20%, visualized as the offset of solid data from EMT predictions for randomly oriented ellipsoidal nanoplatelets in Figure 4, is unaccounted by EMT.

The failure of EMT suggests that the assumptions of the model are not valid through phase change. One possible contributing factor is that graphite nanoplatelets actually increase the thermal conductivity of the surrounding base material, thus making the k_{Solid}/k_{Liquid} ratio appear larger. The molecular dynamics simulations of Babaei *et al.* predict that the presence of graphitic nanoparticles in an octadecane base increases the molecular alignment parameter from 0.15 to 0.91. Babaei *et al.* noted that this alignment parameter in turn has a strong effect on thermal conductivity, with octadecane solid thermal conductivity varying from 0.30 to 1.13 W/m-K for alignment parameters between 0.15 and 0.99.[29] A second factor is that the nanoparticle network experiences a morphological change due to ice-templating that puts the nanoparticles into better contact and reduced separation through nanoplatelet alignment. The potential increase due to alignment of the MLG nanoplatelets is quantified by the Nan *et al.* model, and the prediction shown in Figure 4 is in reasonable agreement with data. While electrical conductivity is extremely sensitive to the freezing rate due to ice-templating, the thermal conductivity is less sensitive, as k_{NC}/k_{Base} of solid samples does not have a clear trend *versus* cooling rate (Figure 4).

CONCLUSION

To conclude, this study of MLG nanoplatelet nanocomposites has observed that electrical conductivity, thermal conductivity, and ice-templating microstructure are tunable through the freezing rate. The nanocomposite has a tunable $\sigma_{Solid}/\sigma_{Liquid}$ ratio that spans over 4 orders of magnitude with the freezing rate, which we hypothesize is caused by ice-templating, whereby nanoplatelets are driven away from the solid–liquid interface and concentrated in the intercrystal regions. The variation of the thermal conductivity with freezing rate cannot be fully explained by the hexadecane freezing rate dependence, as the nanocomposite thermal conductivity contrast ratio and solid phase enhancement follow trends contrary to effective medium theory. We suggest this additional enhancement through freezing is due to ice-templating, consistent with our electrical measurements, as well as nanoparticle-induced molecular alignment of hexadecane.

MATERIALS AND METHODS

Sample Preparation. All liquid nanoparticle suspensions and nanocomposite measurements were performed on freshly prepared mixtures of hexadecane and MLG nanoplatelets. Liquid phase exfoliated MLG nanoplatelets (XG Science XGnP-25) were exposed to an ultraviolet light source (Spectroline model XX-15A UV 365 nm with two BLE-1800B lamps) for 20 min and were then dispersed into hexadecane at 1 vol % in 10 mL batches (the Raman spectra before and after UV exposure are in Supporting Information Figure S4). Sonication was performed with a Fischer Scientific 550 tip sonicator with a 1/8 in. microtip at an amplitude setting of 2 for 60 min. After sonication the average nanoplatelet dimensions were 1–2 μm diameter and 4–10 nm thickness, as verified by atomic force microscopy and transmission electron microscopy (Supporting Information Figure S5).

Freezing Method. The nanocomposites were frozen and tested in an acrylic channel with built-in electrical conductivity and thermal conductivity probes (shown in the Supporting Information S6). The bottom of the acrylic holder is 300 μm thick and was placed into direct contact with a Peltier cooler or a liquid nitrogen bath (for the highest freezing rates). Nanocomposite and pure hexadecane samples were cooled from room temperature (24 °C) with a Peltier cooler at rates between 0.003 and 0.4 °C/min or with a liquid nitrogen bath between 19 and 74 °C/min (Figure 1a). The fastest cooling (74 °C/min) was performed with the liquid nanocomposite in an aluminum channel that precluded electrical conductivity measurement. These freezing rates are based on the slope of the temperature decrease with time, about a 3 °C window centered at the freezing point of hexadecane (17.8 °C).

Electrical and Thermal Conductivity Measurements. Electrical conductivity (σ) is measured between two aluminum plates on opposite sidewalls of the vessel. The conductance is solved for in this simple geometry by $\sigma = L/RA$, where L is the separation between the parallel plates and A is the wetted surface area of the parallel plates. MATLAB software coordinated the control of the Peltier device and measurements of the electrical and thermal conductivity.

Thermal conductivity was measured with a transient hot wire that was initially benchmarked with measurements of liquid water and glycerol.[37] Transient hot wire involves Joule heating a thin platinum wire with a Heavyside function and measuring the wire's resulting temperature rise as a function of time. The wire temperature is sensed through the wire's temperature dependence of electrical resistance, *i.e.*, the thermoresistance. The thermal conductivity of the surrounding medium dictates the wire's temperature rise and is accurately described by an analytical solution to the heat diffusion

equation for line heating of an infinite medium. This solution can be manipulated to isolate thermal conductivity k in terms of the volumetric heating per length of wire q and the rate of temperature rise (ΔT) *versus* the natural log of time (ln t) since the beginning of the Heavyside function,[37]

$$k = \frac{q/4\pi}{\mathrm{d}\Delta T/\mathrm{d}\ln t} \tag{3}$$

To extract thermal conductivity, we determine $\mathrm{d}\Delta T/\mathrm{d}\ln t$ from experimental data, as shown in Figure 1b. As is typically done with transient hotwire, we use a truncated data set spanning the time range of 0.4 to 1.5 s as marked in Figure 1b. At lesser times the heat capacity of the metal wire itself may influence ΔT, while at greater times the thermal response may be influenced by the vessel boundaries or natural convection. We note that the thermal penetration depth ($(4kt/C)^{1/2}$, where C is the volumetric heat capacity) at 1.5 s is only 1.2 mm for the highest k sample, while the distance from the wire to the vessel floor is much greater (4 mm).

Our implementation of this technique uses a 25.4 μm diameter platinum wire of length 40 mm coated in a 2.0 μm Isonel insulation coating (A-M Systems). The current Heavyside function is delivered by the source-side of the Sourcemeter 2400, which joule heats the wire. Simultaneously, the Sourcemeter 2400 sense-side directly measures the voltage across the wire *versus* time. Uncertainties in the measurements were based on observed variability between samples and measurements, as well as systematic uncertainties used in the input parameters (*i.e.*, resistance, thermoresistance, wire diameter, wetted area) used to infer the values of electrical and thermal conductivity from the experiments. The uncertainty is 10% for the electrical conductivity and 2% for the thermal conductivity.

Effective Medium Theory. We compare our results to the EMT model proposed by Nan *et al.* for oriented oblate ellipsoidal particles:[34]

$$\frac{k_{NC}}{k_{Base}} = \frac{2+\phi[\beta_{11}(1-L_{11})(1+\langle\cos^2\theta\rangle)+\beta_{33}(1-L_{33})(1-\langle\cos^2\theta\rangle)]}{2-\phi[\beta_{11}L_{11}(1+\langle\cos^2\theta\rangle)+\beta_{33}L_{33}(1-\langle\cos^2\theta\rangle)]} \tag{4}$$

where k_{NC} is the nanocomposite thermal conductivity, k_{Base} is the base matrix thermal conductivity, k_{NP} is the nanoparticle thermal conductivity, ϕ is the MLG volume fraction, $L_{11} = (p^2)/(2(p^2-1)) + p/(2(1-p^2)^{3/2})\cos^{-1}p$, $L_{33} = 1 - 2L_{11}$, p is the aspect ratio of the thickness to length $p = a_3/a_1$, $\beta_{ii} = (k_{ii}^C - k_{Base})/(k_{Base} + L_{ii}(k_{ii}^C - k_{Base}))$, $\langle\cos^2\theta\rangle = (\int\rho(\theta)\cos^2\theta\sin\theta\,\mathrm{d}\theta)/(\int\sin\theta\,\mathrm{d}\theta)$, $k_{ii}^C = k_{NP}/(1+(1+2p)(1/(h_{TBC}a_3)L_{ii}k_{NP}))$, and h_{TBC} is the thermal boundary conductance. The model shown in Figures 2b and 4 assumes a nanoparticle that is 1 μm $\times$ 7 nm at 1 vol % with k_{NP} = 300 W/m-K,[38] and an assumed thermal boundary conductance h_{TBC} is 12 MW/m^2-K based on the experimentally measured interface between carbon nanotubes and water.[39] We note that the model results here are insensitive to increases in k_{NP} and to the value of h_{TBC} in the range predicted by simulations of various graphene and CNT nanocomposites.[39−41]

Conflict of Interest: The authors declare no competing financial interest.

Acknowledgment. This material is based upon work supported by the National Science Foundation under Grant No. 1209752, the Japanese Society for the Promotion of Science Summer Institute 2012, the AFOSR YIP FA9550-11-1-0030, the Japan Science and Technology Agency through CREST, and the Japanese Government Monbukagakusho (MEXT) Scholarship for S.H. Acknowledgment is made to the donors of the American Chemical Society Petroleum Research Fund for partial support of this research PRF51423DN10. A part of this work was financially supported by Grants-in-Aid for Scientific Research (22226006, 25107002) and JST SICORP, and was conducted in the Research Hub for Advanced Nano Characterization at The University of Tokyo, supported by the Ministry of Education, Culture, Sports, Science and Technology, Japan. We would also like to acknowledge useful discussions with C. Pistorius, A. J.H. McGaughey, and Y. Rabin.

Supporting Information Available: Plot of nanocomposite and hexadecane thermal conductivity *versus* cooling rate; plot of nanocomposite electrical conductivity *versus* cooling rate; environmental scanning electron microscopy of the nanocomposite; Raman spectra of pristine and UV-exposed MLG nanoplatelets; scanning electron microscopy image of presonicated graphite MLG nanoplatelets and tunneling electron microscopy image of postsonicated MLG nanoplatelets; schematic and picture of the experimental setup. This material is available free of charge *via* the Internet at http://pubs.acs.org.

REFERENCES AND NOTES

1. Zhai, Y.; Dou, Y.; Zhao, D.; Fulvio, P. F.; Mayes, R. T.; Dai, S. Carbon Materials for Chemical Capacitive Energy Storage. *Adv. Mater.* **2011**, *23*, 4828–4850.
2. Biener, J.; Stadermann, M.; Suss, M.; Worsley, M. A.; Biener, M. M.; Rose, K. A.; Baumann, T. F. Advanced Carbon Aerogels for Energy Applications. *Energy Environ. Sci.* **2011**, *4*, 656–667.
3. Wu, Q.; Xu, Y.; Yao, Z.; Liu, A.; Shi, G. Supercapacitors Based on Flexible Graphene/Polyaniline Nanofiber Composite Films. *ACS Nano* **2010**, *4*, 1963–1970.
4. Zheng, R.; Gao, J.; Wang, J.; Chen, G. Reversible Temperature Regulation of Electrical and Thermal Conductivity Using Liquid−Solid Phase Transitions. *Nat. Commun.* **2011**, *2*, 289-1–6.
5. Khodadadi, J. M.; Fan, L.; Babaei, H. Thermal Conductivity Enhancement of Nanostructure-Based Colloidal Suspensions Utilized as Phase Change Materials for Thermal Energy Storage: A Review. *Renewable Sustainable Energy Rev.* **2013**, *24*, 418–444.
6. Kedl, R. J. *Wallboard with Latent Heat Storage for Passive Solar Applications*; Technical Report ORNL/TM-11541; Oak Ridge National Lab: Oak Ridge, TN, 1991.
7. Alawadhi, E. M.; Amon, C. H. PCM Thermal Control Unit for Portable Electronic Devices: Experimental and Numerical Studies. *IEEE Trans. Compon., Packag. Technol.* **2003**, *26*, 116–125.
8. Vesligaj, M. J.; Amon, C. H. Transient Thermal Management of Temperature Fluctuations during Time Varying Workloads on Portable Electronics. *IEEE Trans. Compon., Packag. Technol.* **1999**, *22*, 541–550.
9. Sun, P. C.; Wu, Y. L.; Gao, J. W.; Cheng, G. A.; Chen, G.; Zheng, R. T. Room Temperature Electrical and Thermal Switching CNT/Hexadecane Composites. *Adv. Mater.* **2013**, *25*, 4938–4943.
10. Wang, Y.; Tang, B.; Zhang, S. Single-Walled Carbon Nanotube/Phase Change Material Composites: Sunlight-Driven, Reversible, Form-Stable Phase Transitions for Solar Thermal Energy Storage. *Adv. Funct. Mater.* **2013**, *23*, 4354–4360.
11. Harish, S.; Ishikawa, K.; Chiashi, S.; Shiomi, J.; Maruyama, S. Anomalous Thermal Conduction Characteristics of Phase Change Composites with Single-Walled Carbon Nanotube Inclusions. *J. Phys. Chem. C* **2013**, *117*, 15409–15413.
12. Sanusi, O.; Warzoha, R.; Fleischer, A. S. Energy Storage and Solidification of Paraffin Phase Change Material Embedded with Graphite Nanofibers. *Int. J. Heat Mass Transfer* **2011**, *54*, 4429–4436.
13. Chintakrinda, K.; Weinstein, R. D.; Fleischer, A. S. A Direct Comparison of Three Different Material Enhancement Methods on the Transient Thermal Response of Paraffin Phase Change Material Exposed to High Heat Fluxes. *Int. J. Therm. Sci.* **2011**, *50*, 1639–1647.
14. Xu, J.-Z.; Chen, T.; Yang, C.-L.; Li, Z.-M.; Mao, Y.-M.; Zeng, B.-Q.; Hsiao, B. S. Isothermal Crystallization of Poly(l-lactide) Induced by Graphene Nanosheets and Carbon Nanotubes: A Comparative Study. *Macromolecules* **2010**, *43*, 5000–5008.
15. Li, L.; Li, C. Y.; Ni, C. Polymer Crystallization-Driven, Periodic Patterning on Carbon Nanotubes. *J. Am. Chem. Soc.* **2006**, *128*, 1692–1699.
16. Yu, A.; Ramesh, P.; Itkis, M. E.; Bekyarova, E.; Haddon, R. C. Graphite Nanoplatelet−Epoxy Composite Thermal Interface Materials. *J. Phys. Chem. C* **2007**, *111*, 7565–7569.

17. Yavari, F.; Fard, H. R.; Pashayi, K.; Rafiee, M. A.; Zamiri, A.; Yu, Z.; Ozisik, R.; Borca-Tasciuc, T.; Koratkar, N. Enhanced Thermal Conductivity in a Nanostructured Phase Change Composite Due to Low Concentration Graphene Additives. *J. Phys. Chem. C* **2011**, *115*, 8753–8758.
18. Shahil, K. M. F.; Balandin, A. A. Graphene–Multilayer Graphene Nanocomposites as Highly Efficient Thermal Interface Materials. *Nano Lett.* **2012**, *12*, 861–867.
19. Yoonessi, M.; Gaier, J. R. Highly Conductive Multifunctional Graphene Polycarbonate Nanocomposites. *ACS Nano* **2010**, *4*, 7211–7220.
20. Liang, Q.; Yao, X.; Wang, W.; Liu, Y.; Wong, C. P. A Three-Dimensional Vertically Aligned Functionalized Multilayer Graphene Architecture: An Approach for Graphene-Based Thermal Interfacial Materials. *ACS Nano* **2011**, *5*, 2392–2401.
21. Walker, L. S.; Marotto, V. R.; Rafiee, M. A.; Koratkar, N.; Corral, E. L. Toughening in Graphene Ceramic Composites. *ACS Nano* **2011**, *5*, 3182–3190.
22. Deville, S.; Saiz, E.; Nalla, R. K.; Tomsia, A. P. Freezing as a Path to Build Complex Composites. *Science* **2006**, *311*, 515–518.
23. Elgafy, A.; Lafdi, K. Effect of Carbon Nanofiber Additives on Thermal Behavior of Phase Change Materials. *Carbon* **2005**, *43*, 3067–3074.
24. Chen, L.; Zou, R.; Xia, W.; Liu, Z.; Shang, Y.; Zhu, J.; Wang, Y.; Lin, J.; Xia, D.; Cao, A. Electro- and Photodriven Phase Change Composites Based on Wax-Infiltrated Carbon Nanotube Sponges. *ACS Nano* **2012**, *6*, 10884–10892.
25. Goli, P.; Legedza, S.; Dhar, A.; Salgado, R.; Renteria, J.; Balandin, A. A. Graphene-Enhanced Hybrid Phase Change Materials for Thermal Management of Li-ion Batteries. *J. Power Sources* **2014**, *248*, 37–43.
26. Goyal, V.; Balandin, A. A. Thermal Properties of the Hybrid Graphene-Metal Nano-Micro-Composites: Applications in Thermal Interface Materials. *Appl. Phys. Lett.* **2012**, *100*, 073113-1–4.
27. Wei, C. Structural Phase Transition of Alkane Molecules in Nanotube Composites. *Phys. Rev. B: Condens. Matter Mater. Phys.* **2007**, *76*, 134104-1–10.
28. Yang, J.-S.; Yang, C.-L.; Wang, M.-S.; Chen, B.-D.; Ma, X.-G. Crystallization of Alkane Melts Induced by Carbon Nanotubes and Graphene Nanosheets: A Molecular Dynamics Simulation Study. *Phys. Chem. Chem. Phys.* **2011**, *13*, 15476–15482.
29. Babaei, H.; Keblinski, P.; Khodadadi, J. M. Thermal Conductivity Enhancement of Paraffins by Increasing the Alignment of Molecules through Adding CNT/Graphene. *Int. J. Heat Mass Transfer* **2013**, *58*, 209–216.
30. Wilde, G.; Perepezko, J. H. Experimental Study of Particle Incorporation during Dendritic Solidification. *Mater. Sci. Eng., A* **2000**, *283*, 25–37.
31. Stankovich, S.; Dikin, D. A.; Dommett, G. H. B.; Kohlhaas, K. M.; Zimney, E. J.; Stach, E. A.; Piner, R. D.; Nguyen, S. T.; Ruoff, R. S. Graphene-Based Composite Materials. *Nature* **2006**, *442*, 282–286.
32. Rampi, M. A.; Whitesides, G. M. A Versatile Experimental Approach for Understanding Electron Transport through Organic Materials. *Chem. Phys.* **2002**, *281*, 373–391.
33. Hamilton, R. L.; Crosser, O. K. Thermal Conductivity of Heterogeneous Two-Component Systems. *Ind. Eng. Chem. Fundam.* **1962**, *1*, 187–191.
34. Nan, C.; Birringer, R.; Clarke, D. R.; Gleiter, H. Effective Thermal Conductivity of Particulate Composites with Interfacial Thermal Resistance. *J. Appl. Phys.* **1997**, *81*, 6692–6699.
35. Minnich, A.; Chen, G. Modified Effective Medium Formulation for the Thermal Conductivity of Nanocomposites. *Appl. Phys. Lett.* **2007**, *91*, 073105-1–3.
36. Ordonez-Miranda, J.; Yang, R.; Alvarado-Gil, J. J. On the Thermal Conductivity of Particulate Nanocomposites. *Appl. Phys. Lett.* **2011**, *98*, 233111-1–3.
37. Nagasaka, Y.; Nagashima, A. Simultaneous Measurement of the Thermal-Conductivity and the Thermal-Diffusivity of Liquids by the Transient Hot-Wire Method. *Rev. Sci. Instrum.* **1981**, *52*, 229–232.
38. Balandin, A. A. Thermal Properties of Graphene and Nanostructured Carbon Materials. *Nat. Mater.* **2011**, *10*, 569–581.
39. Huxtable, S. T.; Cahill, D. G.; Shenogin, S.; Xue, L.; Ozisik, R.; Barone, P.; Usrey, M.; Strano, M. S.; Siddons, G.; Shim, M.; *et al*. Interfacial Heat Flow in Carbon Nanotube Suspensions. *Nat. Mater.* **2003**, *2*, 731–734.
40. Shenogin, S.; Xue, L.; Ozisik, R.; Keblinski, P.; Cahill, D. G. Role of Thermal Boundary Resistance on the Heat Flow in Carbon-Nanotube Composites. *J. Appl. Phys.* **2004**, *95*, 8136–8144.
41. Hu, L.; Desai, T.; Keblinski, P. Thermal Transport in Graphene-Based Nanocomposite. *J. Appl. Phys.* **2011**, *110*, 033517-1–5.